# Printed Microfluidics

*Christopher Dixon, Julian Lamanna, and Aaron R. Wheeler**

**Microfluidics has become an important tool that is useful for a wide range of applications. A drawback for microfluidics is that many of the techniques that are commonly used to fabricate devices are not widely accessible, not scalable to high-volume manufacturing processes, or both. Recently, a number of printing strategies that were originally developed for other applications have been applied to microfluidic device fabrication. These techniques, which include inkjet printing (IJP), screen printing (SP), and solid wax printing (SWP), are proposed to have a transformative effect on the field. Here microfluidics and printing, are introduced and a list of favorite examples is provided that highlights the accessibility and scalability that the combination is bringing to the field.**

## 1. Introduction

Microfluidics is a family of technologies that manipulates tiny volumes of fluid (femtoliter to microliter) in devices with micrometer-dimension features. Microfluidics has been used for an incredibly diverse array of applications in the fields of chemistry,[1,2] biochemistry,[3–5] molecular diagnostics,[6–8] and microelectronics,[9] among others. Microfluidic systems offer a number of advantageous properties such as low cost, reduced reagent and sample volumes, miniaturized device dimensions, portability, and improved analysis times over comparable macroscale techniques.

Microfluidic device formats can be sub-categorized in numerous ways.[1,8] Here, rather than attempting to comprehensively review all types of microfluidics, we feature three common microfluidic modalities–continuous flow microfluidics (CFM),[10] paper microfluidics, (PM),[11] and digital microfluidics (DMF).[12] CFM is the oldest and most established type of microfluidics in use today, with its roots in gas chromatography[13] and capillary electrophoresis.[14] In CFM devices (**Figure 1**a), liquids are pumped through open channels (in a continuous flow or as a multiphase emulsion of droplets within a carrier fluid[15]) such that they may be merged and mixed with other reagents,[16] interact with species adsorbed to surfaces within the microchannel,[17] or be manipulated by channel geometry to filter and/or concentrate particles.[18] Devices may be simple with a single inlet, channel, and outlet, or incredibly complex, including hundreds of channels, pumps, and valve components that, together, enable applications that were previously impossible.[19] In PM devices (Figure 1b), hydrophilic and porous paper-based substrates are patterned with hydrophobic materials to form virtual "channels" analogous to the physical microchannels found in CFM. The resulting structures are sometimes known as microfluidic paper-based analytical devices (μPADs).[20] Unlike standard CFM devices, fluid flow in PM devices or μPADs is usually passive–it is transported (or "wicked") through the absorptive paper media by capillary action. There is great interest in the use of PM and μPADs for portable applications, benefitting from the fact that these techniques do not require external instrumentation,[20] are compatible with long-term, stable storage of dried reagents,[21] and have very low manufacturing costs.[22] Finally, in contrast to CFM and PM, DMF (Figure 1c) does not feature channels or continuous flows of liquid. In DMF, microliter- to picoliter-sized liquid droplets are manipulated on an open surface using electrostatic forces. In its most common format, droplets in DMF are sandwiched between a counter-electrode top plate and a bottom plate bearing an array of insulated driving electrodes. Individual droplets serve as micro-reactors that can be dispensed, mixed, merged, and separated, making DMF a powerful sample handling and chemical processing technique. The most unique feature of DMF is its re-configurability–a generic device architecture can be used and re-used for virtually unlimited combinations of operations.[23]

Microfluidics (whether implemented in CFM-, PM-, DMF-format, or others) has become an important and widely used tool-set. But a key limitation remains–many of the most interesting variants of these devices require fabrication facilities that are not widely accessible and/or require processes that are not scalable for high-volume manufacturing. While the "accessibility gap" has been recognized and partially addressed by soft lithography[24] and other creative techniques,[25,26] the problem persists, primarily because the most accessible methods are often not directly scalable for mass production. Printing technologies have recently emerged as a robust solution to this problem, making microfluidics widely accessible in a format that is directly scalable for manufacturing. This revolution has been on-going for several years; in fact, do Lago and others

C. Dixon, J. Lamanna, Prof. A. R. Wheeler
Department of Chemistry
University of Toronto
80. St. George Street, Toronto, Ontario M5S 3H6, Canada
E-mail: aaron.wheeler@utoronto.ca
J. Lamanna, Prof. A. R. Wheeler
Donnelly Centre for Cellular and Biomolecular Research
University of Toronto
160 College Street, Toronto, Ontario M5S 3E1, Canada
Prof. A. R. Wheeler
Institute for Biomaterials and Biomedical Engineering
University of Toronto
164 College Street, Toronto, Ontario M5S 3G9, Canada

**DOI: 10.1002/adfm.201604824**

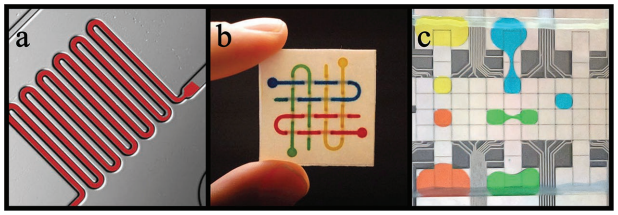


**Figure 1.** Microfluidic modalities. (a) Continuous flow microfluidics (CFM). In CFM, fluids are moved within closed micrometer-dimension channels, driven via external pumps interfaced with inlets and outlets in the chip. Reproduced with permission from Prof. Samuel Sia, Columbia University. (b) Paper microfluidics (PM). Hydrophobic/hydrophilic patterns form "channels" in paper substrates and fluid flow is driven by capillary forces. Reproduced with permission from Dr. Andres Martinez, Whitesides Research Group, Harvard University. (c) Digital microfluidics (DMF). Discrete picoliter to microliter-sized droplets of liquid are manipulated on an array of electrodes using electrostatic forces.

have used laser printing to form microchannels for interesting applications for more than a decade.[27–29] More recently, 3D printing has emerged as a popular motif for forming microfluidic devices, interconnects, and components.[30–33] In this review, we have chosen to focus on the three printing strategies that we propose are transforming the field of microfluidics: inkjet printing, screen printing, and solid wax printing.

Inkjet printing (IJP) (**Figure 2**a, top) is one of the most ubiquitous printing technologies in the consumer market. In IJP, ink droplets are deposited by liquid flow (rather than pressure) onto digitally configurable locations on a substrate.[34] IJP was traditionally used to deposit colored inks, but more recently the technology has been adapted to deposit a wide range of materials including metals, ceramics, polymers, chemical reagents,[34] proteins,[35] tissues,[36] hydrogels[37] and living cells.[38,39] The high precision, high spatial resolution, simplicity, and ease of preparation of IJP make it particularly attractive for the formation of fine patterns of such materials in microfluidic devices. In the most common IJP drop-on-demand format, droplets are generated by either a thermal[40] or piezoelectric[41] inkjet print head (Figure 2a, middle). In the latter format a piezoelectric element (PE) is placed upon a flexible diaphragm which in turn contacts a chamber filled with ink. An electric pulse is applied to the PE causing it to deform, compressing the ink chamber and ejecting a droplet of ink through the nozzle and onto the substrate beneath. The resulting ink droplets can combine to create photo-quality images with resolutions of up to several thousand dots per inch (i.e., tens to hundreds micrometers).[34]

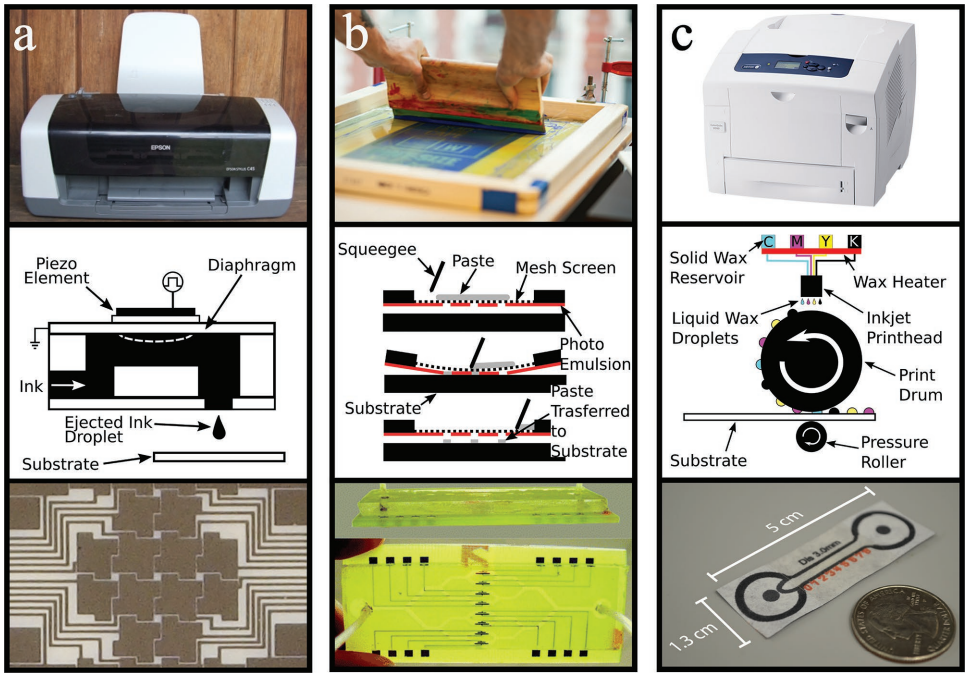


**Figure 2.** Printing methods used for microfluidic device fabrication. (a) (Top) Photo of a consumer inkjet printer, adapted from wikimedia.org under Creative Commons license attribution. (Middle) Cartoon (not to scale) schematic of a piezoelectric inkjet print head. Ink from a reservoir fills a chamber topped with a piezoelectric element fixed above a flexible diaphragm. A waveform is applied to the piezoelectric element deforming the chamber and forcing a droplet of ink onto the substrate. (Bottom) Photo of inkjet-printed electrodes in a digital microfluidic (DMF) device. Reproduced with permission.[42] Copyright 2016, the Royal Society of Chemistry. (b) (Top) Photo of a screen printing apparatus, adapted from wikimedia.org under Creative Commons license attribution. (Middle) Cartoon (not to scale) schematic of the SP process. An ink paste is pressed into a mesh screen that sits atop a developed photo-emulsion mask. A squeegee is used to transfer the paste to the substrate forming patterned structures. (Bottom) Photo of screen-printed channels and electrochemical electrodes in a microfluidic device. Reporduced with permission.[46] Copyright 2007, the Royal Society of Chemistry. (c) (Top) Photo of a commercial wax printer, adapted from wikimedia.org under Creative Commons license attribution. (Middle) Cartoon (not to scale) schematic of the wax printing process. Solid wax [colored cyan (C), magenta (M), yellow (Y), or black (K)] is melted in a heater before passing through an inkjet printing head onto a rotating print drum. Droplets on the drum are then transferred to the substrate as it passes between the print drum and pressure roller. (Bottom) Photo of a wax-printed microfluidic device. Reproduced with permission.[50] Copyright 2014, the Royal Society of Chemistry.

The bottom panel of Figure 2a is a photo showing a portion of a DMF device produced using an inkjet printer to form silver electrodes.[42] IJP can also be used to pattern hydrophobic inks on porous paper-based substrates to generate the microfluidic channels found in μPADs.[43]

Screen printing (SP) (Figure 2b, top) is a pressure-based printing technology most commonly associated with the production of clothing and other wares.[44] Like IJP, SP has recently emerged as a useful tool for printed electronics and microfluidics because of its ability to produce patterned layers of diverse materials.[45] The middle panel of Figure 2b features a cartoon highlighting the SP process. To create printed patterns, a photo-emulsion mask is first developed that is the negative image of the pattern to be created. This mask is then placed between a mesh screen attached to a frame and the substrate to be patterned. A paste-like ink is then applied to the screen and with pressure from a squeegee, the resulting image is transferred to the substrate. The bottom panel of Figure 2b features a photo of a proof-of-concept microfluidic device with screen-printed electroanalytical electrodes. The device also features screen-printed microchannel walls formed by repeated printing and drying of a UV curable dielectric paste using thick-film SP technology.[46]

Solid wax printing (SWP) (Figure 2c, top) is the newest of the three printing technologies featured in this review; the first commercial product was introduced by Tektronix® in 1991.[47] Similar to IJP and SP, SWP was initially used for other applications, but has recently been repurposed to form microfluidic devices such as μPADs.[48,49] SWP has advantages over other techniques such as negligible ink drying times (i.e., the molten wax solidifies upon contact with the cool substrate), fabrication methods that require only a few steps (i.e., design, print, post-bake), and the capacity to form wax-printed sheets that can be fed into an inkjet printer to form SWP-IJP hybrid devices.[11,49] A simplified representation of the SWP process is depicted in the middle panel of Figure 2c (not to scale). Inside the printer, solid wax cubes are melted with an integrated heater and the molten wax is transported to an inkjet print head where it is deposited onto the printing drum. The substrate material is then fed in between a pressure roller and the printing drum, transferring the image to the substrate where it cools and solidifies on the surface of the paper. To create PM channels, the substrate must be heated such that the wax again becomes molten and penetrates through the thickness of the paper, forming a hydrophobic barrier to the hydrophilic channels. The bottom panel of Figure 2c features a wax-printed μPAD used for isotachophoretic sample focusing.[50]

**Table 1.** Microfluidic Structures Formed with Printing Technologies.

| Printing Technology | CFM Channel Walls | PM Channel Barriers | Electrodes (for DMF and other applications) |
|---|---|---|---|
| Inkjet Printing | – | +[51] | +[52,53] |
| Screen Printing | +[46] | +[44] | +[54,55] |
| Solid Wax Printing | – | +[49,50] | – |

As noted, the printing technologies of IJP, SP, and SWP have recently been used to form microfluidic devices in the CFM-, PM-, and DMF-formats; specifics are summarized in **Table 1**.

In choosing a printing method, the user should consider those specifics, as well as the printed feature size, substrate throughput, and cost. Those variables are often inter-related; for example, a consumer-grade desktop ink-jet printer (≈100 $) can generate printed features in the 150-400 μm range,[42,53] while an industry-grade ink-jet system such as the Dimatix (Fujifilm, Santa Clara, CA) line of printers (≈50 000$) can generate printed features in the sub-100 μm range.[52,56] Depending on the application, the cost of the latter may well be worth it, given its tremendous customizability (owing to the capacity of the user to control the piezoelectric dispensing conditions), with great flexibility in reagent compatibility, drop size and spacing, print heights, print temperatures, and print waveforms. Similarly, start-up costs should be also considered when choosing a printing method. While IJP and SWP allow for printing directly from a design, SP requires the acquisition of a mask. On the other hand, after obtaining a mask, the throughput of SP is higher than the alternate techniques. Figures for printed feature size, instrument cost, start-up cost, printed layer thickness, and throughput are summarized in **Table 2**.

Microfluidic devices formed by IJP, SP, and SWP have been used for diverse applications, ranging from molecular diagnostics[62,63] to drug screening.[64,65] Here, we have chosen to highlight a few of our favorite examples of printed microfluidic devices, organized around three popular application-areas for the technology: immunoassays, applications involving biological cells, and environmental applications. These examples are not comprehensive, serving instead to illustrate the variety of creative ways that researchers are using printed microfluidics to solve a wide range of problems.

**Table 2.** Characteristics of Printing Technologies.

| Printing Technology | Minimum Printed Feature Size (μm) | Instrument Cost[a)] | Relative Start-up Cost[b)] | Printed Layer Thickness (μm) | High Throughput Printing |
|---|---|---|---|---|---|
| Inkjet Printing | ≈150-400 [42,53] | $ | Low | 0.2-20[57,58] | – |
| | ≈20-100 [52,56] | $$$ | | | |
| Screen Printing | ≈200-1800 [44,45] | $ | High | 0.4-300[46,59] | + |
| | ≈40-150 [60] | $$$ | | | |
| Solid Wax Printing | ≈850 [49] | $$ | Low | 6-14[61] | – |

[a)]$: ≈100 $; $$ ≈1000 $; $$$: ≥50 000 $; [b)]Start-up cost includes both time and financial cost (aside from the instrument, ink, and printing media) invested prior to first print.

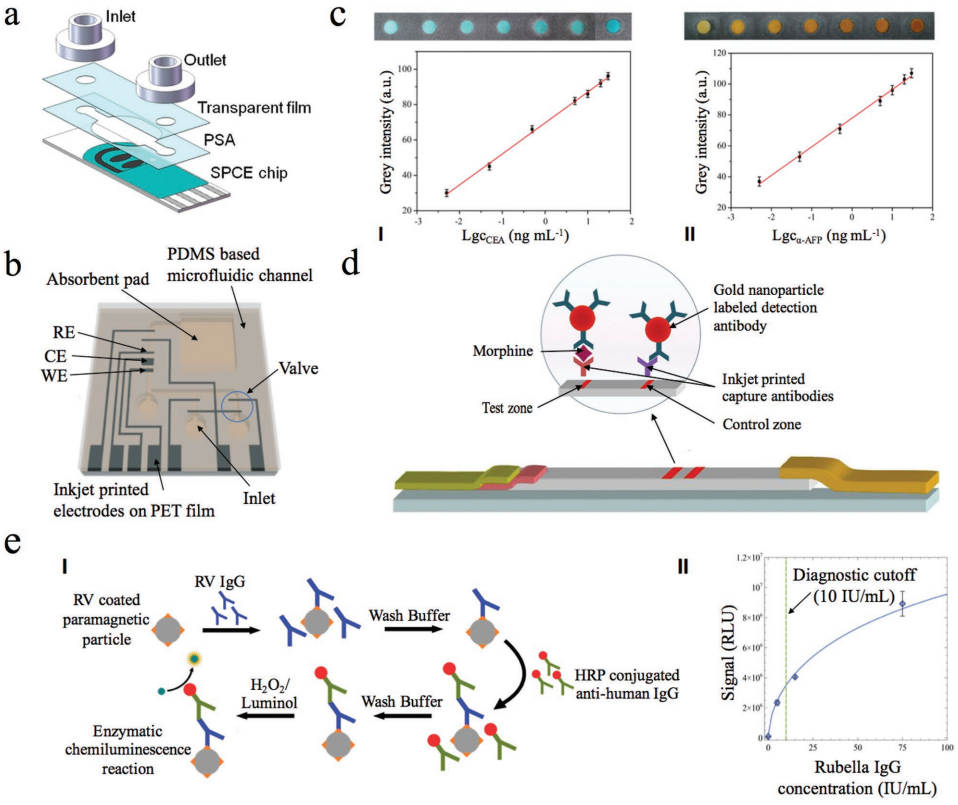


**Figure 3.** Immunoassays in printed microfluidic systems. (a) Schematic of a three-layer CFM device with screen-printed carbon electrodes used to detect tumor necrosis factor alpha (TNF$\alpha$). The bottom layer comprises a screen-printed carbon electrode (SPCE) chip. The middle layer includes an open chamber formed from pressure sensitive adhesive (PSA). The top layer (enclosing the chamber and the electrodes) was formed from a transparent film. Inlet and outlet ports facilitated introduction of samples and reagents into the CFM device. Reproduced with permission.[67] Copyright 2015, Elsevier. (b) Schematic of a CFM device with inkjet-printed silver electrodes used to detect Salmonella in an amperometric immunoassay. The device comprises a polyethylene terephthalate (PET) film with inkjet-printed silver electrodes mated to a polydimethylsiloxane (PDMS) based network of microfluidic channels. The design features 3 inlets designated for 10 µL aliquots of Salmonella-containing sample solution, washing buffer, and enzymatic substrate. Electrowetting valves were used to control the flow, which was driven by an absorbent wicking pad at the outlet. The electrochemical cell includes an inkjet-printed gold counter electrode (CE), working electrode (WE), and silver reference electrode (RE). Reproduced with permission.[68] Copyright 2015, the Royal Society of Chemistry. (c) Pictures illustrating colorimetric response (top) and calibration curves plotted on a logarithmic scale (concentrations of 0.005, 0.05, 5, 10, 20 and 30 ng mL$^{-1}$, bottom) for (I) carcinoembryonic antigen (CEA) and (II) $\alpha$-fetoprotein ($\alpha$-AFP) detected using a solid wax-printed PM device. Error bars represent ± 1 standard deviation for n = 11 replicates. Reproduced with permission.[73] Copyright 2015, Elsevier. (d) Schematic diagram depicting the assembly of a PM lateral flow test with inkjet-printed capture antibodies (light red, test zone) and control antibodies (purple, control zone). An aqueous sample containing morphine (maroon diamonds) is transported through the paper by capillary flow where the morphine is immobilized on the test zone. Captured morphine is then visualized upon binding of gold nanoparticle labeled detection antibody on the test zone (and as a positive control, the same reporter binds to control zone). Reproduced with permission.[78] Copyright 2014, Springer-Verlag Berlin Heidelberg. (e) Inkjet-printed digital microfluidic (DMF) device – (I) Cartoon illustrating the many steps of a chemiluminescent immunoassay implemented on an inkjet-printed DMF device. Magnetic particles coated with inactivated rubella virus (RV) (orange) are used to capture the analyte, RV IgG (blue), and secondary antibodies (green) conjugated to horse radish peroxidase (HRP) (red) convert luminol and $H_2O_2$ into a chemiluminescent product (turquoise). (II) Calibration curve for RV IgG detection on a printed DMF device. The chemiluminescent signal is plotted as a function of RV IgG concentration, highlighting the cutoff for diagnosis (10 IU mL$^{-1}$). Error bars represent ± 1 standard deviation for n = 3 replicates. Reproduced with permission.[42] Copyright 2016, the Royal Society of Chemistry.

## 2. Immunoassays

The immunoassay exploits antibody-antigen interactions for the detection of analytes in biological samples. This application has been popular in the microfluidics community for decades building from the recognition that automated, integrated, and miniaturized immunoassay systems are particularly useful as portable tests at the point of care (POC).[66] Each of the printing modalities (IJP, SP, and SWP) and microfluidic formats (CFM, PM, and DMF) covered here have been explored in this area for several years (in a variety of creative arrangements), suggesting that mature techniques suitable for widespread use are on the horizon. We describe several of our favorite examples below.

The use of CFM devices with printed sensing parts is particularly attractive for the development of low-cost and fully disposable immunosensing devices. For example, Eletxigerra et al.[67] developed a disposable microfluidic device with commercial screen printed carbon electrodes (SPCE) (**Figure 3**a) for the detection of the inflammation biomarker, tumor necrosis factor alpha (TNF$\alpha$) (CFM, SP). The electrodes were functionalized

with antibodies using a straightforward physical adsorption procedure, allowing for the subsequent capture and detection of TNF$\alpha$. Microfluidic channels were formed on top of the screen-printed electrodes using a pressure sensitive adhesive and transparency film, which were mated with home-made syringe ports. Screen printing the electrodes allowed for devices to be formed rapidly with high inter-batch reproducibility. Further, the low cost of the electrodes and other substrates allowed for the production of cost-effective microfluidic devices, such that they were fully disposable, an improvement over traditional (non-disposable) approaches involving the enzyme-linked immunosorbent assay (ELISA), the gold standard for TNF$\alpha$ detection.[67]

Chen et al.[68] demonstrated how the use of printing techniques can enable the mass production and commercial viability of a microfluidic biosensor (Figure 3b) (CFM, IJP). The authors fabricated microchannels in a polyethylene terephthalate (PET) substrate using nanoimprint lithography.[69] Samples containing salmonella were evaluated on-chip by exposing them to antibody-conjugated magnetic beads as the first step in an electrochemical ELISA. Fluids were transported through the microchannels by capillary action, with timing controlled by inkjet-printed electrowetting valves.[70] The latter are particularly innovative (without moving parts), taking advantage of surface energy differences–the electrodes are coated with hydrophobic 1H,1H,2H,2H-perfluorodecanethiol (PFDT), which initially prevents fluid flow; upon application of a voltage, the surface energy increases, allowing fluid to pass. IJP was also used to fabricate the three-electrode system used to carry out the electrochemical measurements. The printing processes used for fabrication of this biosensor are straightforward to extend to a roll-to-roll format,[71,72] enabling the potential for low-cost, high-volume manufacturing, a key benchmark for commercial microfluidic POC applications.

A representative example of a multiplexed immunoassay performed on a printed PM substrate is described in Liang et al.[73] (Figure 3c) (PM, SWP). In this work, a colorimetric method was used for the quantitative detection of two tumour markers, carcinoembryonic antigen (CEA) and $\alpha$-fetoprotein ($\alpha$-AFP), using an "origami" inspired µPAD. SWP was used to define sensing areas on a top sheet comprising a central sample loading zone integrated to PM channels leading to three antibody capture zones, and a bottom sheet featuring three matching observation windows for colorimetric readout. This device benefitted from the large surface area of the fibers making up the paper, which allowed for the formation of a flower-like gold nanoparticle network [which served as the substrate for the capture antibodies for CEA and $\alpha$-AFP (top sheet)]. In practice, as sample wicked through the network, analytes were captured in the sensing areas and then detected using secondary antibodies conjugated to a chemically stable peroxidase analog. The bottom sheet was folded to meet the top sheet such that in the presence of the substrates, different colors with different intensities (corresponding to differing concentrations of CEA and $\alpha$-AFP) were visualized and quantified through the observing windows of the bottom sheet. CEA and $\alpha$-AFP were detected over a linear range of 0.005 to 30 ng mL$^{-1}$ with a limit of detection (LOD) of 1.7 pg mL$^{-1}$ for both analytes, results comparable to reference values from a commercial ELISA method (CEA and $\alpha$-AFP concentrations above 3.5 ng mL$^{-1}$[74] and 30 ng mL$^{-1}$[75] respectively may indicate increased cancer risk). Choosing SWP to define sensing areas allowed for the use of a paper platform and corresponding immunoassay that was non-toxic and low-cost (when compared to other fabrication methods), demonstrating its potential for POC diagnostics.

As noted in the introduction, PM represents an extension of lateral flow assay (LFA) techniques, which historically relied on nitrocellulose as the absorptive medium for fluid wicking.[76,77] In the more recent PM literature, nitrocellulose (which is flammable and suffers from batch-to-batch reproducibility challenges) has largely been replaced with cellulose-based paper substrates. For example, Teerinen et al.[78] demonstrated the utility of cellulose paper as an analytical membrane for LFA-detection of morphine (Figure 3d) (PM, IJP). The authors noted that it was important to consider a number of factors when designing a LFA, including paper pore size (flow rate), non-specific interactions with the cellulose fibers, and immobilization of sufficient amounts of test and control antibodies. A Dimatix inkjet printer was used to print anti-morphine and anti-human antibodies at the test and control zones respectively, allowing for targeted, low-volume use of reagents (1 µg per spot). When assembled, the devices were useful for quantifying morphine levels in under 20 minutes, and a LOD of 20 ng/mL in oral fluid (cut-off level 40 ng /mL$^{-1}$ in this matrix[79]) was achieved, demonstrating the sensitivity of this platform for performing assays in clinically relevant ranges.

Finally, DMF is emerging as an alternative technology to PM and CFM for performing low cost immunoassays. While DMF devices have been used for a wide range of applications,[12] they were until very recently fabricated using photolithography and other cleanroom-based techniques to pattern and coat electrodes on glass or silicon substrates. Recently, DMF joined CFM and PM in benefitting from cleanroom-free IJP fabrication techniques.[42,52,53] For example, Dixon et al.[42] demonstrated that fully functional DMF devices could be fabricated on flexible substrates using IJP (DMF, IJP). Silver electrodes were printed onto a paper-like substrate and used to perform a 13-step rubella virus (RV) IgG immunoassay (Figure 3e). A four-point calibration curve was generated with a LOD of 0.2 IU mL$^{-1}$, well below the diagnostic cut-off of 10 IU mL$^{-1}$ for this assay. Further, the use of the IJP platform and flexible substrates allowed for processing on a roll-coater (a first for DMF), allowing for formation of integrated devices for <1$. Roll-coating serves as an intermediate step in the progression to roll-to-roll high-volume manufacturing.[80]

## 3. Applications Involving Biological Cells

Laboratory work with biological cells is typically implemented by manual or automated techniques. The former (manual techniques) are low-throughput, time-consuming, and labor-intensive, but make use of relatively inexpensive disposables such as microtiter well plates, petri dishes, and cell culture flasks. The latter (automated methods) use (often prohibitively) expensive liquid handling robots, but allow for automated, high-throughput and parallel-scale processing, eliminating the time and labor issues outlined above.[81] Microfluidic techniques

have emerged as a "medium throughput," "quasi-automated" alternative to the existing methods, and exploratory work in this area has been extensively reported in the literature. IJP (applied to patterning cells and materials) and SP (applied to forming electrochemical detectors) have been used for many years to form CFM devices to culture and analyze cells. More recently, wax-printed PM devices have been proposed as an alternate scheme for cell culture and analysis. Several examples of printed CFM methods and one example of a printed PM device are described below.

A key step in many microfluidic applications involving cells is cell trapping, sorting, and manipulation. Printed CFM devices have recently been applied for this purpose. For example, Wee et. al[54] used screen-printed electrodes to manipulate cardiac fibroblast cells by dielectrophoresis (DEP) (**Figure 4**a) (CFM, SP). The microfluidic devices used in this work comprised screen-printed silver (Ag) electrodes covered with a poly(methyl methacrylate) (PMMA) substrate containing an integrated microchannel. In a second example, Zhu et al.[55] reported DEP-based trapping of yeast cells in CFM chips formed by thick-film SP (Figure 4b) (CFM, SP). CFM channels as well as interdigitated carbon electrodes and contact wires were screen-printed onto a glass substrate, and in a proof-of-principle experiment, yeast cells were separated from polystyrene beads. The low cost of the screen-printed electrodes in the examples above is important; traditionally, DEP electrodes have been formed using expensive cleanroom-based techniques, but experiments with cells often limit devices to a single use before disposal.[82] A third method for cell trapping in printed microfluidic devices was reported by Chen et al.,[83] who isolated circulating tumour cells (CTCs) from whole blood using an inkjet-printed CFM device (Figure 4c) (CFM, IJP). To form these devices, a Dimatix printer was used to deposit clusters of magnetic nanoparticles onto glass slides (each cluster comprising a micromagnet). Microchannels were interfaced to this substrate, and were used to deliver blood from which the CTCs were captured. Prior to analysis, samples were mixed with a ferrofluid containing nanoparticles (NPs) functionalized with CTC-specific antibodies. CTC-NP complexes were attracted to the micromagnets relative to other cell types such as red blood cells (RBCs) and white blood cells (WBCs). These three examples highlight the utility of printed microfluidic devices for cell trapping in experiments involving a wide range of cell types, demonstrating the flexibility of devices formed using SP and IJP.

CFM devices are useful for trapping cells and carrying out cell-based assays, but they can also be used as components in printers, themselves. For example, Zhang et al.[84] developed a custom IJP instrument relying on CFM with modifiable printing parameters and the ability to print and pattern multiple biocompatible materials (Figure 4d) (CFM, IJP). Traditional inkjet printers have had limited use in cell printing because they lack the ability to eject droplets of viscous materials (e.g., cells in sodium alginate) and they typically require that high voltages be applied to the printing heads, which can damage the cells. The custom inkjet printer described here addresses these limitations, allowing cells to be printed from inkjet channels with relatively low voltages (40 V) applied to the printing heads. The new system also allowed for multiple cell types to be printed with precise spatial control, allowing for the development of methods that are more efficient and less labor intensive than conventional cell analysis experiments.

A key driver in the application of CFM technologies to biological cells has been the potential to form cell culture systems with integrated, real-time metabolic monitoring. Printed CFM devices have recently been applied for this purpose; for example, McKenzie et al.[85] developed a CFM platform for the detection of glucose, lactate, oxygen and pH (Figure 4e) (CFM, SP and IJP). The multi-analyte detection was enabled using five screen-printed platinum (Pt) electrodes which were further modified by IJP enzymes and polymer films. The devices were used to collect real-time metabolic measurements in on-chip macrophage culture for each of the four analytes, before and after cell death. The planar screen-printed electrodes simplified the design of the microfluidics, and the flexibility of the fabrication method allows for rapid reconfiguration and modification with a wide variety of enzymes, polymers, and metal films, depending on the type of sensor required.

Finally, PM devices have recently been applied to integrated cell culture and analysis. In conventional cell culture systems, cells are adhered to a flat surface, referred to as two-dimensional (2D) cell culture. However, this is not always an accurate model for the three-dimensional (3D) space that many cells experience in living systems. Tao et al.[86] developed a paper-based 3D PM cell culture system (Figure 4f, I) for the analysis of cell proliferation and chemosensitivity with SWP-defined culturing areas and fluidic channels in cellulose filter paper (PM, SWP). Cell proliferation measurements (Figure 4f, II) in the PM system, determined by absorbance measurements, indicated no significant differences compared to traditional, hydrogel-based 3D model systems. Additionally, the authors noted that the use of hydrogel-free PM devices allowed for more straightforward evaluation by alternate techniques such as scanning electron microscopy (SEM).

## 4. Environmental Applications

The ability to monitor contaminants and pollutants in the environment is of utmost importance for public health. Typically, environmental monitoring requires low detection limits–parts per million (ppm) and parts per billion (ppb), which often requires complex methodologies and large, expensive instruments.[87] The use of microfluidic devices formed using printing techniques has the potential to address the growing need for portable low-cost environmental monitoring. There are a few examples of CFM systems in this area, but the majority of work has been implemented in PM format, making use of IJP, SP, and SWP to deposit sensing elements and reagents, define sensing areas, and form electrodes and sensors. Examples are described below.

Although PM is the most commonly used platform for performing environmental applications, there are a few examples of CFM devices being used for this purpose. For example, Calvo-Lopez et al.[88] developed a credit-card-sized CFM platform (**Figure 5**a) for the potentiometric determination of ammonium ions from water samples (CFM, SP). Reagents and samples were injected into the device via a peristaltic pump and

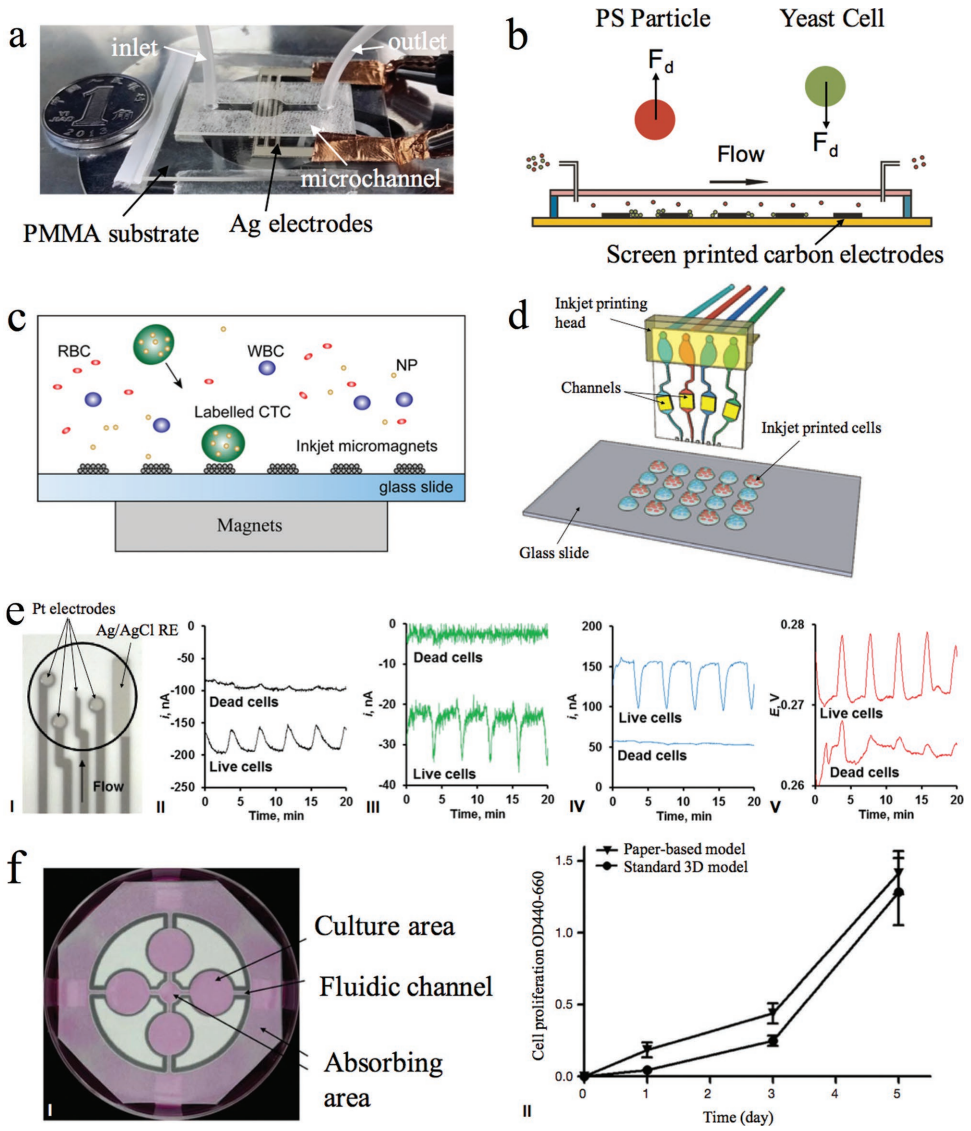


**Figure 4.** Applications involving biological cells in printed microfluidic systems. (a) Photograph of a CFM chip with screen-printed silver (Ag) electrodes used for dielectrophoretic (DEP) cell trapping experiments. The CFM substrate is formed from polymethylmethacrylate (PMMA), which is mated to inlet and outlet ports. Reproduced with permission.[54] Copyright 2015, IOP Publishing. (b) Schematic illustrating the separation of yeast cells (green) from a mixture of cells and polystyrene (PS) particles (red) in a screen-printed CFM DEP chip. As the mixture moves through the channel, yeast cells are pulled toward the electrodes by positive DEP forces ($F_d$) while PS particles are repelled from the electrodes by negative DEP. Reproduced with permission.[55] Copyright 2015, Elsevier. (c) Schematic portraying the principle of immunomagnetic circulating tumor cell (CTC, green) separation on a CFM chip with integrated inkjet-printed micromagnets. Samples are mixed with a ferrofluid which includes magnetic nanoparticles (NPs, yellow) functionalized with antibodies. The NPs specifically bind CTCs, which are pulled toward the micromagnets relative to other cell types such as red blood cells (RBCs, red) and white blood cells (WBCs, purple) inside the channel. Reproduced with permission.[83] Copyright 2016, Biomedical Engineering Society. (d) Schematic of a custom inkjet printer used to deposit hepatoma cells HepG2 (red) and glioma cells U251 (blue) on a glass substrate. Reproduced with permission.[84] Copyright 2016, the Royal Society of Chemistry. (e) (I) Picture of platinum screen-printed electrodes used for multianalyte detection [as well as an Ag/AgCl reference electrode (RE)] in a CFM device (the arrow indicates the direction of flow) applied to cell culture with integrated analysis of metabolites. Graphs featuring real-time detection of (II) glucose (black), (III) lactate (green), (IV) oxygen (blue), and (V) pH (red) in macrophage culture at inkjet-printed sensors in a CFM device. Current (i) and potential (E) signals were obtained before and after cell death and recorded as a function of time. Reproduced with permission.[85] Copyright 2015, American Chemical Society. (f) (I) Photo of a PM culture system with SWP-defined fluidic channels and absorbing and cell culturing areas used for studying cell proliferation and chemosensitivity. (II) Graph of cell proliferation for cells cultured in the PM system (triangles) and a standard 3D system (circles). Cells were seeded and cultured for 5 days and cell proliferation was quantified by absorbance of water-soluble tetrazolium salt (WST). Error bars represent ± 1 standard deviation for n = 3 replicates. Reproduced with permission.[86] Copyright 2015, the Korean BioChip Society and Springer-Verlag Berlin Heidelberg.

six-way injection valve, delivered through the microchannels to a polyvinylidene fluoride (PVDF) gas diffusion membrane, and ammonium ions were detected potentiometrically using an ammonium selective working electrode. SP was chosen for fabricating the silver/silver chloride reference electrode to allow for precise positioning of the electrode within the

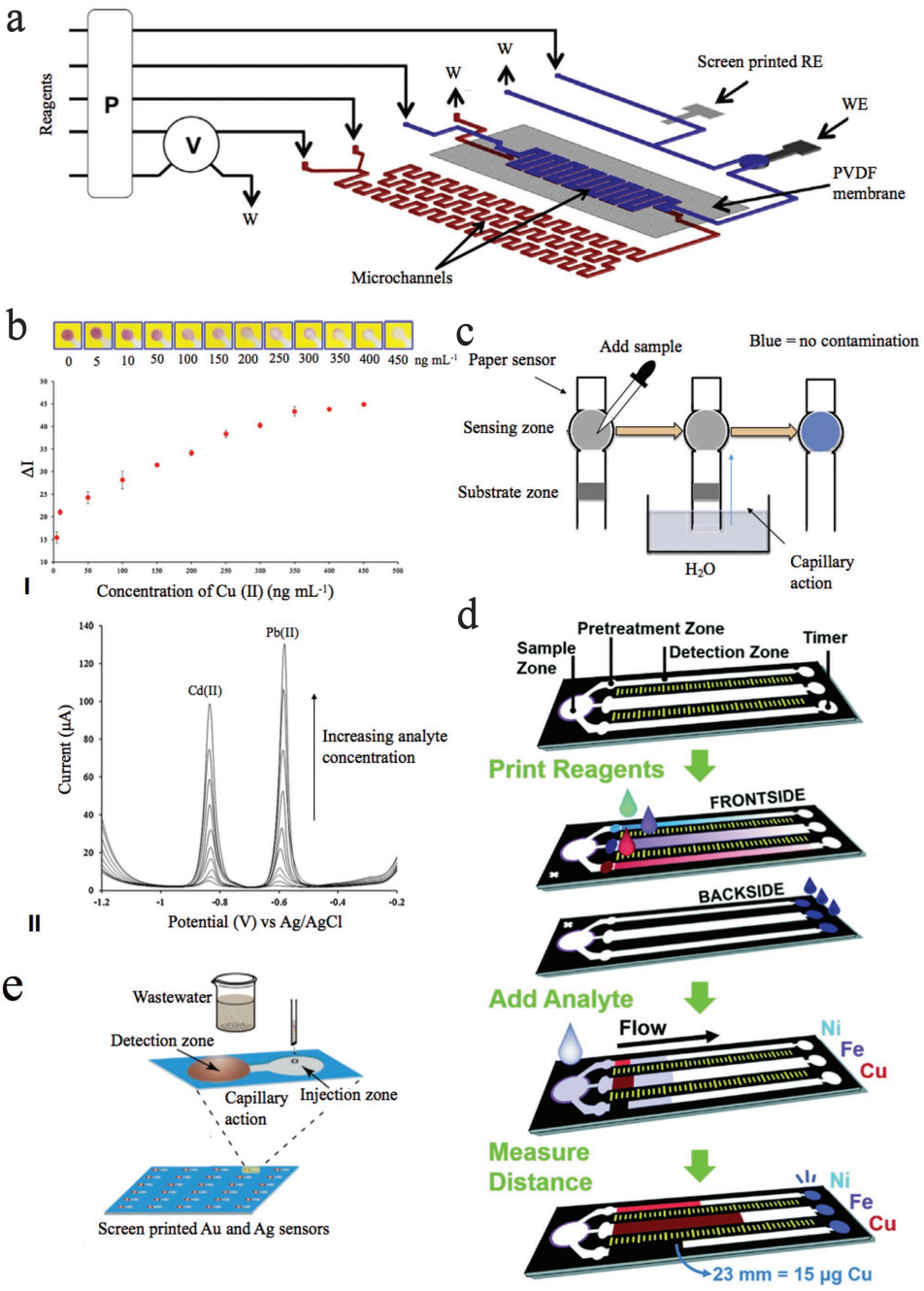


**Figure 5.** Environmental applications in printed microfluidic systems. (a) Schematic of a CFM device used to detect ammonium ions in water samples using a screen-printed silver/silver chloride reference electrode (RE) and an ammonium-selective working electrode (WE). Reagents and samples were injected into the device via a peristaltic pump (P) and six-way injection valve (V), delivered through the microchannels (red), and through the polyvinylidene fluoride (PVDF) membrane (blue), where they were detected potentiometrically and carried to the waste outlet (W). Reproduced with permission.[88] Copyright 2015, Elsevier. (b) (I) Pictures illustrating colorimetric response (top) and intensity plot (bottom) for copper (Cu) (II) detected using a solid wax-printed μPAD. The mean changes in intensities are plotted as a function of Cu(II) concentration. Error bars represent ± 1 standard deviation for n = 3 replicates. (II) Anodic stripping voltammograms of cadmium (Cd) (II) and lead (Pb) (II) measured at a SP-fabricated electrochemical cell in the same μPAD. Reproduced with permission.[93] Copyright 2016, Elsevier. (c) Schematic of a PM device used to analyze organophosphates in water samples. The sensing and substrate zones were defined by SWP and included inkjet-printed layered structures of cationic polymer/sol–gel silica/acetylcholinesterase (AChE)/sol–gel silica and sol–gel silica/indoxyl acetate/sol–gel silica respectively. The sample is added to the sensing zone and water ($H_2O$) is used to transport the substrate, indoxyl acetate, through the PM device by capillary action. When there is no contamination, AChE hydrolyzes the substrate into a blue product. Reproduced with permission.[95] Copyright 2015, Elsevier. (d) Schematic illustrating the use of a μPAD with solid wax-printed channels and inkjet-printed reagents in an experiment quantifying nickel (Ni), copper (Cu) and iron (Fe) concentrations in air borne particulate matter. Analytes were added to the sample zone and transported via capillary action through a pretreatment zone and a detection zone for

microfluidic channel. This work demonstrated that a miniaturized, disposable, simple and selective CFM device could be used for the detection of ammonium ions at a LOD of 0.07 ± 0.01 mg $L^{-1}$. The LOD for the CFM device is below that reported for a microfluidic device fabricated by traditional soft lithography and wet etching techniques[89] and is below 0.2 mg $L^{-1}$, the natural ammonium ion concentration in water as determined by the World Health Organization.[90]

The most established microfluidic format for simple and low cost environmental analysis is the PM/μPAD, in which quantitative readout is often accomplished via colorimetric and electrochemical methods.[91,92] For example, Chaiyo et al.[93] combined SWP and SP techniques to fabricate a μPAD to detect lead (Pb)(II), cadmium (Cd)(II) and copper (Cu)(II) (PM, SWP and SP). SWP was used to define zones for colorimetric and electrochemical detection as well as reference color zones and channels, and SP was used to form an electrochemical cell comprising a carbon counter electrode (CE) and silver/silver chloride reference electrode (RE) (all used with a working electrode not formed by SP). Cu(II) was detected by colorimetric methods (Figure 5b, I) with a LOD of 64.8 nM, which is well below 20 μM, the maximum allowable level in water in the United States.[94] Pb(II) and Cd(II) were detected electrochemically (Figure 5b, II) with LODs of 0.48 nM and 0.89 nM, which are significantly lower than the World Health Organization's limits in water of 48.3 nM and 24.1 nM respectively.[90] In summary, SWP and SP were instrumental in allowing for the development of a sensor with dual detection modalities (electrochemical and colorimetric) in an inexpensive and highly sensitive platform.

A drawback of colorimetric detection techniques is the requirement for using bulky detectors and optics, which often limits their use in portable detectors. In an attempt to address this limitation, Sicard et al.[95] developed a colorimetric detector that relies on a smartphone for determining organophosphate pesticide concentrations in water samples (Figure 5c) (PM, SWP and IJP). SWP was used to define the sensor areas (sensing and substrate zone) and IJP was used to print layered structures comprised of cationic polymer/ sol–gel silica/acetylcholinesterase (AChE)/ sol–gel silica at the sensing zone and a sol–gel silica/indoxyl acetate/ sol–gel silica at the substrate zone. A second benefit (in addition to small size) of the smartphone detector was internet-enabled transmission of results, demonstrating promise for remote sensing in the field. Cate et al.[48] developed an alternative system to solve the problem of bulky detectors and optics for field-testing (PM, SWP and IJP). Their μPAD was fabricated by SWP and IJP for the multiplexed detection of nickel (Ni), copper (Cu) and iron (Fe) particulates from atmospheric samples (Figure 5d). A clever distance-based detection system (where longer distance means higher amount) was developed, which allows for rapid quantitation by eye (advantageous over traditional methods that rely on external readers[96]). The multiplexed technique had time-weighted average values for aerosol exposure monitoring of 71.3-784, 14.3-927, and 71.3-927 μg $m^{-3}$ which are within the permissible exposure limits of 1000, 100, and 1000 μg $m^{-3}$ for Ni, Cu, and Fe, respectively.[97] Printing of reagents provided great device reproducibility, high reagent patterning resolution, and minimal reagent waste compared to manual deposition methods such as pipetting.

Finally, an alternative to colorimetric and electrochemical detection methods is surface enhanced Raman scattering (SERS), which offers ultrasensitive analysis with high selectivity. For example, Qu et al.[98] reported the use of gold (Au) and silver (Ag) sensors fabricated on cellulose paper by SP for the detection of substituted aromatic pollutants (benzidine, pyrocatechol, aniline, and *p*-aminobenzoic acid) in wastewater samples (Figure 5e) (PM, SP). The SP technique enabled high-volume fabrication of the sensors, which were embedded in a simple paper substrate. As wastewater wicked through the devices, particles (which could potentially interfere with the analysis) were trapped, allowing for the water and analytes to reach the sensors unimpeded. The low cost and passive nature of these sensors makes them particularly well-suited for portable analysis of pollutants in the field.

## 5. Conclusion and Outlook for the Future

As described herein, microfluidics has become important across a wide range of disciplines, having particular impact in immunoassays, applications involving biological cells, and environmental applications. The advantages of microfluidics for these (and many other) applications are compelling; however, for widespread adoption, device fabrication processes must become accessible and scalable such that they are compatible with high-volume manufacturing. Here, we have highlighted three technologies that are bridging this gap: inkjet printing (IJP), screen printing (SP), and solid wax printing (SWP). These techniques each have advantages and disadvantages, such that they are useful in complementary applications (sometimes in tandem). For example, IJP is well suited for forming electrodes and for modifying device surfaces with high-resolution patterns of reagents and biological materials (whether for CFM, PM, or DMF). IJP is also particularly well suited for rapid prototyping, as it is does not require a mask for each design iteration. Screen printing, while also being capable of forming electrodes, suffers from reduced resolution, larger minimum feature sizes, and requires a mask for each design. But SP (uniquely) is useful for forming microchannel walls, and the throughput of SP makes it attractive for high-volume manufacturing. Finally, given the importance of PM/μPAD/LFA techniques for portable

Ni, Cu, and Fe. The distance travelled in the detection zone was correlated to amount of analyte, and could thus be used for quantitation. A blue dye was inkjet-printed on the backside of the device, functioning as a timer to indicate the completion of the assay. When the sample reached the end of the detection zone, the printed blue dye was resolubilized, indicating completion of the assay. Reproduced with permission.[48] Copyright 2015, the Royal Society of Chemistry. (e) Schematic depicting pollutant detection in wastewater samples using a μPAD with screen-printed gold (Au) and silver (Ag) sensors. The sample is applied to the injection zone and transported to the detection zone via capillary action through a cellulose substrate, where the pollutants are detected by surface-enhanced Raman spectroscopy. Reproduced with permission.[98] Copyright 2013, Elsevier.

analysis, SWP is a critically important technology for economical fabrication of such devices, which are being applied to a wide range of applications. We believe that SWP fabricated PM devices have great potential for performing portable, low-cost, rapid diagnostic tests compatible with mass manufacturing.

In summary, we propose that printing has begun to revolutionize microfluidics, and that the years to come will see a proliferation of inexpensive roll-to-roll processing that will bring this promising technology to ever greater numbers of users. This will benefit us all, with beneficial effects on human health, cell biology research, environmental monitoring, and beyond.

## Acknowledgements

C.D. and J.L. contributed equally to this work. The authors thank Abbott Laboratories for funding.

Received: September 16, 2016
Revised: December 5, 2016
Published online: February 6, 2017

[1] K. S. Elvira, X. C. i Solvas, R. C. R. Wootton, A. J. deMello, *Nat. Chem.* **2013**, *5*, 905.
[2] H. Kim, K.-I. Min, K. Inoue, D. J. Im, D.-P. Kim, J.-I. Yoshida, *Science* **2016**, *352*, 691.
[3] D. Kim, X. Wu, A. T. Young, C. L. Haynes, *Acc. Chem. Res.* **2014**, *47*, 1165.
[4] M. Mehling, S. Tay, *Curr. Opin. Biotechnol.* **2014**, *25*, 95.
[5] G. Du, Q. Fang, J. M. J. den Toonder, *Anal. Chim. Acta* **2016**, *903*, 36.
[6] P. N. Nge, C. I. Rogers, A. T. Woolley, *Chem. Rev.* **2013**, *113*, 2550.
[7] K. N. Han, C. A. Li, G. H. Seong, *Annu. Rev. Anal. Chem.* **2013**, *6*, 119.
[8] E. K. Sackmann, A. L. Fulton, D. J. Beebe, *Nature* **2014**, *507*, 181.
[9] S.-S. Li, C.-M. Cheng, *Lab Chip* **2013**, *13*, 3782.
[10] G. M. Whitesides, *Nature* **2006**, *442*, 368.
[11] A. W. Martinez, S. T. Phillips, G. M. Whitesides, E. Carrilho, *Anal. Chem.* **2010**, *82*, 3.
[12] K. Choi, A. H. C. Ng, R. Fobel, A. R. Wheeler, *Annu. Rev. Anal. Chem.* **2012**, *5*, 413.
[13] S. C. Terry, J. H. Jerman, J. B. Angell, *IEEE Trans. Electron Devices* **1979**, *26*, 1880.
[14] D. J. Harrison, K. Fluri, K. Seiler, Z. Fan, C. S. Effenhauser, A. Manz, *Science* **1993**, *261*, 895.
[15] M. T. Guo, A. Rotem, J. A. Heyman, D. A. Weitz, *Lab Chip* **2012**, *12*, 2146.
[16] C.-Y. Lee, C.-L. Chang, Y.-N. Wang, L.-M. Fu, *IJMS* **2011**, *12*, 3263.
[17] N. Annabi, Š. Selimović, J. P. A. Cox, J. Ribas, M. A. Bakooshli, D. Heintze, A. S. Weiss, D. Cropek, A. Khademhosseini, *Lab Chip* **2013**, *13*, 3569.
[18] X. Wang, C. Liedert, R. Liedert, I. Papautsky, *Lab Chip* **2016**, *16*, 1821.
[19] V. Sanchez-Freire, A. D. Ebert, T. Kalisky, S. R. Quake, J. C. Wu, *Nat. Protoc.* **2012**, *7*, 829.
[20] A. W. Martinez, S. T. Phillips, G. M. Whitesides, *Proc. Natl. Acad. Sci. USA* **2008**, *105*, 19606.
[21] G. E. Fridley, H. Q. Le, E. Fu, P. Yager, *Lab Chip* **2012**, *12*, 4321.
[22] X. Li, D. R. Ballerini, W. Shen, *Biomicrofluidics* **2012**, *6*, 11301.
[23] H. Kim, M. J. Jebrail, A. Sinha, Z. W. Bent, O. D. Solberg, K. P. Williams, S. A. Langevin, R. F. Renzi, J. L. Van De Vreugde, R. J. Meagher, J. S. Schoeniger, T. W. Lane, S. S. Branda, M. S. Bartsch, K. D. Patel, *PLOS One* **2013**, *8*, e68988.
[24] Y. Xia, A. G. M. Whitesides, *Annu. Rev. Mater. Sci.* **1998**, *28*, 153.
[25] A. Grimes, D. N. Breslauer, M. Long, J. Pegan, L. P. Lee, M. Khine, *Lab Chip* **2008**, *8*, 170.
[26] C. W. T. Yang, E. Ouellet, E. T. Lagally, *Anal. Chem.* **2010**, *82*, 5408.
[27] C. Lucio do Lago, H. D. Torres da Silva, C. A. Neves, J. G. Alves Brito-Neto, J. A. Fracassi da Silva, *Anal. Chem.* **2003**, *75*, 3853.
[28] W. K. T. Coltro, D. P. de Jesus, J. A. F. da Silva, C. L. do Lago, E. Carrilho, *Electrophoresis* **2010**, *31*, 2487.
[29] F. R. de Souza, G. L. Alves, W. K. T. Coltro, *Anal. Chem.* **2012**, 9002.
[30] A. K. Au, W. Huynh, L. F. Horowitz, A. Folch, *Angew. Chem. Int. Ed.* **2016**, *55*, 3862.
[31] S. Waheed, J. M. Cabot, N. P. Macdonald, T. Lewis, R. M. Guijt, B. Paull, M. C. Breadmore, *Lab Chip* **2016**, *16*, 1993.
[32] C. Chen, B. T. Mehl, A. S. Munshi, A. D. Townsend, D. M. Spence, R. S. Martin, *Anal. Methods* **2016**, *8*, 6005.
[33] S. Y. Lockwood, J. E. Meisel, F. J. Monsma Jr., D. M. Spence, *Anal. Chem.* **2016**, *88*, 1864.
[34] G. D. Martin, I. M. Hutchings, in *Inkjet Technology for Digital Fabrication* (Eds.: I. M. Hutchings, G. D. Martin), John Wiley & Sons, Ltd, Chichester, UK, **2012**, pp. 21–44.
[35] W. C. Wilson, T. Boland, *The Anatomical Record* **2003**, *272A*, 491.
[36] T. Xu, W. Zhao, J.-M. Zhu, M. Z. Albanna, J. J. Yoo, A. Atala, *Biomaterials* **2013**, *34*, 130.
[37] J. T. Delaney, A. R. Liberski, J. Perelaer, U. S. Schubert, *Soft Matter* **2010**, *6*, 866.
[38] T. Xu, J. Jin, C. Gregory, J. J. Hickman, T. Boland, *Biomaterials* **2005**, *26*, 93.
[39] M. Nakamura, A. Kobayashi, F. Takagi, A. Watanabe, Y. Hiruma, K. Ohuchi, Y. Iwasaki, M. Horie, I. Morita, S. Takatani, *Tissue Eng.* **2005**, *11*, 1658.
[40] N. Morita, in *Inkjet-Based Micromanufacturing*, Wiley-VCH Verlag GmbH & Co. KGaA, Weinheim, Germany, **2012**, pp. 41–56.
[41] H. Wijshoff, *Phys. Rep.* **2010**, *491*, 77.
[42] C. Dixon, A. H. C. Ng, R. Fobel, M. B. Miltenburg, A. R. Wheeler, *Lab Chip* **2016**, *16*, 4560.
[43] J. Wang, M. R. N. Monton, X. Zhang, C. D. M. Filipe, R. Pelton, J. D. Brennan, *Lab Chip* **2014**, *14*, 691.
[44] W. Dungchai, O. Chailapakul, C. S. Henry, *Analyst* **2011**, *136*, 77.
[45] M. Yafia, S. Shukla, H. Najjaran, *J. Micromech. Microeng.* **2015**, 1.
[46] H. Dong, C.-M. Li, Y.-F. Zhang, X.-D. Cao, Y. Gan, *Lab Chip* **2007**, *7*, 1752.
[47] C. W. Jaeger, "*Color Solid Ink Printing*," can be found under http://www.imaging.org/ist/resources/tutorials/solid_ink.cfm (accessed Jul 4, 2016).
[48] D. M. Cate, S. D. Noblitt, J. Volckens, C. S. Henry, *Lab Chip* **2015**, *15*, 2808.
[49] E. Carrilho, A. W. Martinez, G. M. Whitesides, *Anal. Chem.* **2009**, *81*, 7091.
[50] T. Rosenfeld, M. Bercovici, *Lab Chip* **2014**, *14*, 4465.
[51] K. Maejima, S. Tomikawa, K. Suzuki, D. Citterio, *RSC Adv.* **2013**, *3*, 9258.
[52] R. Fobel, A. E. Kirby, A. H. C. Ng, R. R. Farnood, A. R. Wheeler, *Adv. Mater.* **2014**, *26*, 2838.
[53] H. Ko, J. Lee, Y. Kim, B. Lee, C.-H. Jung, J.-H. Choi, O.-S. Kwon, K. Shin, *Adv. Mater.* **2014**, *26*, 2335.
[54] W. H. Wee, Z. Li, J. Hu, N. A. Kadri, F. Xu, F. Li, B. Pingguan-Murphy, *J. Micromech. Microeng.* **2015**, *25*, 105015.
[55] H. Zhu, X. Lin, Y. Su, H. Dong, J. Wu, *Biosens. Bioelectron.* **2015**, *63*, 371.
[56] J. Lessing, A. C. Glavan, S. B. Walker, C. Keplinger, J. A. Lewis, G. M. Whitesides, *Adv. Mater.* **2014**, *26*, 4677.
[57] Y. Wang, X. W. Sun, G. K. L. Goh, H. V. Demir, H. Y. Yu, *IEEE Trans. Electron. Devices* **2010**, *58*, 480.

[58] W. J. Tseng, S. Y. Lin, S.-R. Wang, *J Electroceram* **2006**, *16*, 537.
[59] S. E. Shaheen, R. Radspinner, N. Peyghambarian, G. E. Jabbour, *Appl. Phys. Lett.* **2001**, *79*, 2996.
[60] W. J. Hyun, E. B. Secor, M. C. Hersam, C. D. Frisbie, L. F. Francis, *Adv. Mater.* **2014**, *27*, 109.
[61] M. S. Thomas, B. Millare, J. M. Clift, D. Bao, C. Hong, V. I. Vullev, *Ann. Biomed. Eng.* **2009**, *38*, 21.
[62] T. Okamoto, T. Suzuki, N. Yamamoto, *Nat. Biotechnol.* **2000**, *18*, 438.
[63] J. Lu, S. Ge, L. Ge, M. Yan, J. Yu, *Electrochim. Acta* **2012**, *80*, 334.
[64] G. Arrabito, B. Pignataro, *Anal. Chem.* **2010**, *82*, 3104.
[65] P. Chandra, S. A. Zaidi, H.-B. Noh, Y.-B. Shim, *Biosens. Bioelectron.* **2011**, *28*, 326.
[66] A. H. C. Ng, U. Uddayasankar, A. R. Wheeler, *Anal. Bioanal. Chem.* **2010**, *397*, 991.
[67] U. Eletxigerra, J. Martinez-Perdiguero, S. Merino, *Sens. Actuators, B* **2015**, *221*, 1406.
[68] J. Chen, Y. Zhou, D. Wang, F. He, V. M. Rotello, K. R. Carter, J. J. Watkins, S. R. Nugen, *Lab Chip* **2015**, *15*, 3086.
[69] S. Y. Chou, *J. Vac. Sci. Technol. B* **1996**, *14*, 4129.
[70] W. Satoh, H. Yokomaku, H. Hosono, N. Ohnishi, H. Suzuki, *J. Appl. Phys.* **2008**, *103*, 034903.
[71] S. H. Ahn, L. J. Guo, *Adv. Mater.* **2008**, *20*, 2044.
[72] D. Angmo, T. T. Larsen-Olsen, M. Jørgensen, R. R. Søndergaard, F. C. Krebs, *Adv. Energy Mater.* **2012**, *3*, 172.
[73] L. Liang, S. Ge, L. Li, F. Liu, J. Yu, *Anal. Chim. Acta* **2015**, *862*, 70.
[74] A. M. Ballesta, R. Molina, X. Filella, J. Jo, N. Giménez, *Tumor Biol.* **1995**, *16*, 32.
[75] Y. Sato, K. Nakata, Y. Kato, M. Shima, N. Ishii, T. Koji, K. Taketa, Y. Endo, S. Nagataki, *N. Engl. J. Med.* **1993**, *328*, 1802.
[76] C. Chen, J. Wu, *Sensors* **2012**, *12*, 11684.
[77] L. G. Lee, E. S. Nordman, M. D. Johnson, M. F. Oldham, *Biosensors* **2013**, *3*, 360.
[78] T. Teerinen, T. Lappalainen, T. Erho, *Anal. Bioanal. Chem.* **2014**, *406*, 5955.
[79] D. M. Bush, *Forensic Sci. Int.* **2008**, *174*, 111.
[80] H. F. Dam, T. R. Andersen, M. V. Madsen, T. K. Mortensen, M. F. Pedersen, U. Nielsen, F. C. Krebs, *Sol. Energy Mater. Sol. Cells* **2015**, *140*, 187.
[81] A. H. C. Ng, B. B. Li, M. D. Chamberlain, A. R. Wheeler, *Annu. Rev. Biomed. Eng.* **2015**, *17*, 91.
[82] R. C. Gallo-Villanueva, C. E. Rodríguez-López, R. I. Díaz-de-la-Garza, C. Reyes-Betanzo, B. H. Lapizco-Encinas, *Electrophoresis* **2009**, *30*, 4195.
[83] P. Chen, Y.-Y. Huang, G. Bhave, K. Hoshino, X. Zhang, *Ann. Biomed. Eng.* **2016**, *44*, 1710.
[84] J. Zhang, F. Chen, Z. He, Y. Ma, K. Uchiyama, J.-M. Lin, *Analyst* **2016**, *141*, 2940.
[85] J. R. McKenzie, A. C. Cognata, A. N. Davis, J. P. Wikswo, D. E. Cliffel, *Anal. Chem.* **2015**, *87*, 7857.
[86] F. F. Tao, X. Xiao, K. F. Lei, I.-C. Lee, *BioChip J* **2015**, *9*, 97.
[87] N. A. Meredith, C. Quinn, D. M. Cate, T. H. Reilly, J. Volckens, C. S. Henry, *Analyst* **2016**, *141*, 1874.
[88] A. Calvo-López, O. Ymbern, M. Puyol, J. M. Casalta, J. Alonso-Chamarro, *Anal. Chim. Acta* **2015**, *874*, 26.
[89] S. Xue, K. Uchiyama, H.-F. Li, *J. Environ. Sci.* **2012**, *24*, 564.
[90] World Health Organization, *Guidelines for Drinking-Water Quality: Recommendations*, World Health Organization, Geneva, **2004**.
[91] D. M. Cate, J. A. Adkins, J. Mettakoonpitak, C. S. Henry, *Anal. Chem.* **2015**, *87*, 19.
[92] A. K. Yetisen, M. S. Akram, C. R. Lowe, *Lab Chip* **2013**, *13*, 2210.
[93] S. Chaiyo, A. Apiluk, W. Siangproh, O. Chailapakul, *Sens. Actuators, B* **2016**, *233*, 540.
[94] X. Wang, L. Chen, L. Chen, *Microchim. Acta* **2014**, *181*, 105.
[95] C. Sicard, C. Glen, B. Aubie, D. Wallace, S. Jahanshahi-Anbuhi, K. Pennings, G. T. Daigger, R. Pelton, J. D. Brennan, C. D. M. Filipe, *Water Res.* **2015**, *70*, 360.
[96] M. M. Mentele, J. Cunningham, K. Koehler, J. Volckens, C. S. Henry, *Anal. Chem.* **2012**, *84*, 4474.
[97] "*Table Z-1 Limits for Air Contaminants*," can be found under https://www.osha.gov/pls/oshaweb/owadisp.show_document?p_table=STANDARDS&p_id=9992&p_text_version=FALSE (accessed Sep 15, 2016).
[98] L. L. Qu, Q. X. Song, Y. T. Li, M. P. Peng, D. W. Li, L. X. Chen, *Anal. Chim. Acta* **2013**, *792*, 86.